THE FORMATION OF VOIDS IN THE DUCTILE FRACTURE OF A LOW ALLOY STEEL

C Q Zheng* & J C Radon
Imperial College, London, England

DEVELOPMENT OF VOIDS

The process of void formation on the boundaries of the second phase particles is one of the important mechanisms of ductile fracture. Ductile fracture, or rupture occurs by the coalescence of microvoids; it has been investigated by many workers [1]. It occurs in three stages; namely, nucleation, growth and coalescence of voids. In the present work the ductile fracture process was studied using tensile cylindrical specimens made of steel BS4360-50D used widely for the construction of North Sea Oil platforms. The composition, mechanical properties and test methods were reported in previous papers [1,2].

The development of voids in 50D steel can be described as follows. From the beginning of the yielding process up to the plastic strain ε_p of *0.10* the formation of small holes and globular cavities was observed. These voids were typically of a spherical shape. The nucleation of irregularly shaped voids on the boundaries of the second phase particles was less frequent and occurred only at higher strains. Another interesting geometry of voids was the formation of spherical cavities around globular inclusions. The presence of a spherical cavity may strongly influence the progressive development of failure; in this case a sharp crack propagated from a fold in the cavity which had originated in the matrix at a slope of about 45^0. Subsequently larger and more complicated deformations were observed at the higher effective plastic strain ε_p of *0.14*. At this strain level and up to approximately *0.24* a rapid nucleation of a large number of voids was recorded around smaller, usually spheroidal inclusions.

It should be mentioned that the maximum tensile load P_{max} was reached typically at the strain $\varepsilon_p = 0.16$ at the beginning of the necking process [2]. However, it was also observed that with further increases of strain new voids were nucleating continuously, but their subsequent growth was much slower and their number limited.

With further increases of strain from $\varepsilon_p = 0.14$ up to *0.60* and higher, close to the final rupture, the nucleation and the growth of voids was seen to occur around the following inclusions:

MnS, $(CaO)_x.(Al_2O_3)$, CaS, $MnO.FeO$, $Ca_x(Al_2O_3)_y.SiO_2$ and $(MgO)_x.(Al_2O_3)_y$. MnO. These inclusions were analysed in detail and will be described elsewhere.

At strains above $\varepsilon_p = 0.60$ the voids were observed to nucleate around much smaller inclusions, such as Cu particles, not larger than 1.3 μm and this secondary nucleation process deserves particular attention on account of the size of the particles. Other small spheroidal particles were Al_2O_3, again less than 1 μm in diameter, and also small and very regular spheres, less than 0.7 μm diameter of MnS.

It may therefore be concluded that initially and at low strains, the voids developed from the largest inclusions available in a specific stress field. At higher strains, however, the nucleation process transferred to the boundaries of the minor inclusions.

GROWTH OF VOIDS

Once nucleation was completed, the actual growth of the voids was closely related to the increasing plastic strain ε_p. A growth process frequently observed in the strain range between $\varepsilon_p = 0.6$ and *0.7* started from the centrally situated spherical inclusion of the composition $MgO_x.(Al_2O_3)_y$. MnO. Another typical growth process is shown in Figure 1 where an ellipsoidal void formed around the inclusion SiO_2 at a similar strain range as above. Irregular holes grown at similar strains and under the same conditions were also noted. A linear relationship between the relative volumes of voids and the plastic strain ε_p discussed in [2] was again recorded.

COALESCENCE OF VOIDS

The third part of the ductile process, namely the coalescence of voids, was studied in two orientations. It was observed that in the direction of axial loading the coalescence started at strains of *0.6* and in some cases slightly earlier. However, as expected, in the direction perpendicular to the load axis, the coalescence began much later and at higher strains. In some tests the coalescence was observed to start not far from the instability strain amounting to *90%* of the true fracture strain [1,2].

Using the relation ε_p *vs* a/R (the ratio of the radius of minimum cross section of the neck a *vs.* the radius of the profile of the neck R), [1], and the distribution of stresses [3,4] in the minimum section of the necked tensile specimen, the relationship between the triaxial stress state parameter $\sigma_m/\bar{\sigma}$ and ε_p for the unnotched tensile specimen was constructed, Figure 2. Here σ_m is the mean stress and $\bar{\sigma}$ is the effective stress. This function was subsequently used in plotting the relationship of the relative volume of voids V_v and the effective

*Visiting scientist, Northwestern Polytechnical University, Xian, The People's Republic of China

plastic strain ε_p, [2] i.e. the function $\frac{\ln Vv/Vo}{\varepsilon_p - \varepsilon_o}$ vs. $\frac{\sigma_m}{\bar{\sigma}}$ presented as Figure 3. V_o is the relative volume of voids at the beginning of the nucleation process, and ε_o is the effective plastic strain corresponding to V_o. In Figure 3 the results obtained from the tests on A533B steel [5,6] are also included for comparison. Two conclusions may be drawn from this relationship. Firstly, it will be observed that the present results for steel 50 D are very similar to those for steel A 533B, though the results from the tests on steel A 533B were not fully documented. Secondly, the function $\frac{\ln Vv/Vo}{\varepsilon_p - \varepsilon_o}$ for 50 D unnotched specimens decreases suddenly with the increasing ratio $\sigma_m/\bar{\sigma}$ at low stress values, i.e. at $\sigma_m/\bar{\sigma} < 0.5$, then becoming nearly constant at higher stresses of about $\sigma_m/\bar{\sigma} = 0.7$. Finally, it should be noted that with the exception of the lowest stress values recorded ($\sigma_m/\bar{\sigma} = 0.48$), the experimental values from [6] were nearly identical with our data in the investigated range of $\sigma_m/\bar{\sigma}$ from 0.5 to 0.7. However, they are noticeably below the corresponding analytical results [7], which may be explained on the basis that our experimental data represented the combination of the nucleation and the growth of voids in a complicated situation. A typical example of the elongation of an originally spherical shape and subsequent coalescence of the voids in the loading direction is shown in Figure 1. A similar change in the geometry of the voids was observed elsewhere in the necked part of the tensile specimens. Thus the difference between the experimental data and analytical results [7] is not surprising.

REFERENCES

[1] C. Q. Zheng and J. C. Radon, Basic Tensile Properties of A Low-Alloy Steel BS 4360-50D, Presented at International Conf. on Fracture Mechanics Technology applied to material evaluation and structure design in Melbourne, Australia, August 1982. In print.

[2] C. Q. Zheng and J. C. Radon, Tearing Instability and Rupture of A Low-Alloy Steel. December 1982, to be published.

[3] P. W. Bridgman, Studies in Large Flow and Fracture, McGraw-Hill, New York, 1952.

[4] A. C. Mackenzie, T. W. Hancock and D K Brown, On the Influence of state of stress on Ductile Failure Initiation In High Stress Steels, Engineering Fracture Mechanics, 1977, 9, 167-188.

[5] D A Shockey et al, A Computational Fracture Model for SA 533 grade B Class 1 Steel Based upon Microfracture Processes, NP-701 Special Report, Electric Power Research Institute (EPRI), February 1978 8.1 — 8.31.

[6] D A Shockey et al, Computational Modelling of Microstructural Fracture Processes in A533B Pressure Vessel Steel, NP-1398, Final Report, EPRI, May 1980.

[7] J R Rice and P M Tracey, On the Ductile Enlargement of Voids in Triaxial Stress Fields, J. Mech. Phys. Solids, 1969, 17, 201-217.

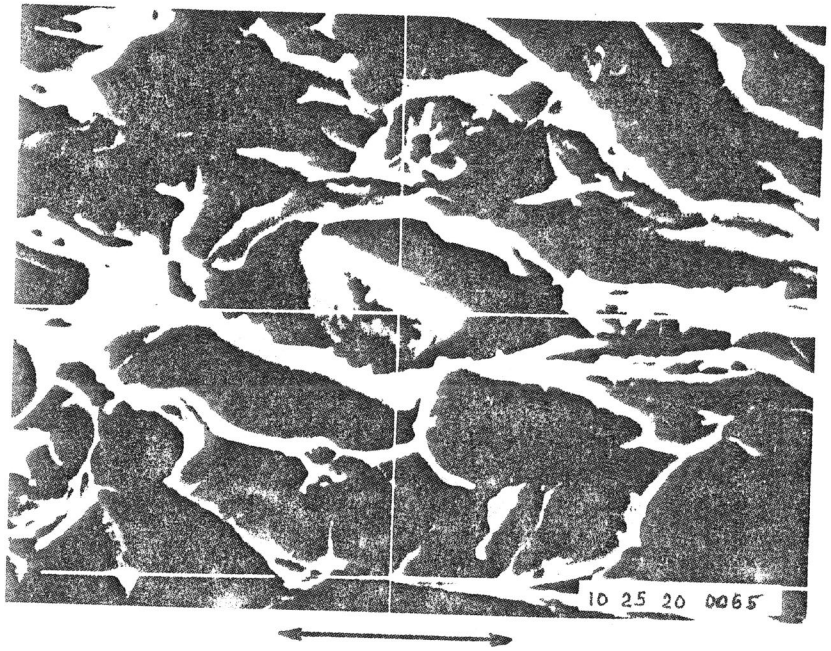

Fig. 1. Steel BS 4360-50 D
Void around SiO_2 inclusion

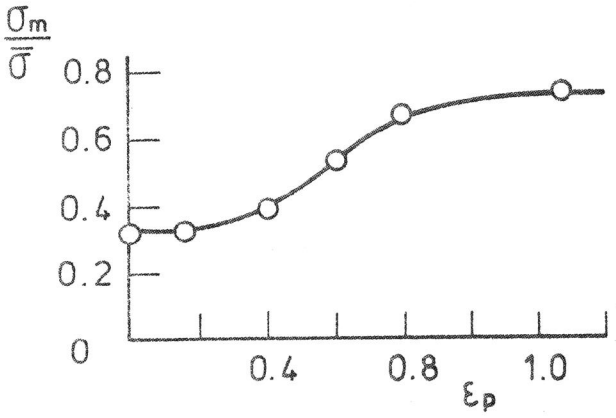

Fig. 2. Steel BS 4360-50D.
$\sigma_m/\bar{\sigma}$ *vs.* ε_p

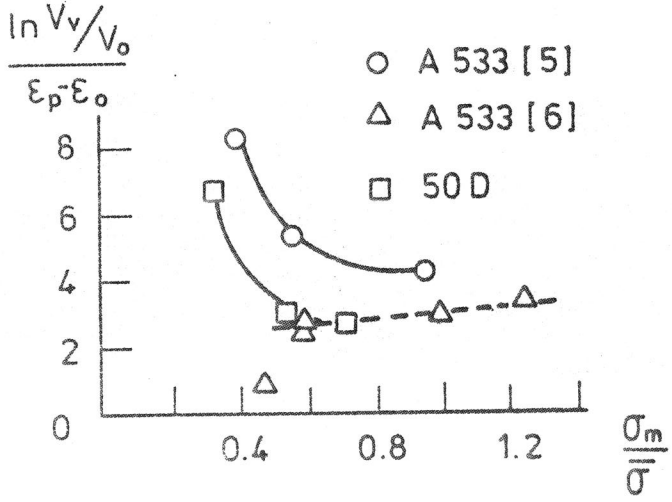

Fig. 3. $\frac{ln\ Vv/Vo}{\varepsilon_p - \varepsilon_o}$ *vs.* $\sigma_m/\bar{\sigma}$